Cell Metabolism
Article

Time-Restricted Feeding without Reducing Caloric Intake Prevents Metabolic Diseases in Mice Fed a High-Fat Diet

Megumi Hatori,[1,4] Christopher Vollmers,[1,4] Amir Zarrinpar,[1,2,4] Luciano DiTacchio,[1,4] Eric A. Bushong,[3] Shubhroz Gill,[1] Mathias Leblanc,[1] Amandine Chaix,[1] Matthew Joens,[1] James A.J. Fitzpatrick,[1] Mark H. Ellisman,[3] and Satchidananda Panda[1,*]

[1]Salk Institute for Biological Studies, La Jolla, CA 92037, USA
[2]Department of Gastroenterology, University of California, San Diego, La Jolla, CA 92037, USA
[3]National Center for Microscopy and Imaging Research, University of California, San Diego, La Jolla, CA 92093, USA
[4]These authors contributed equally to this work
*Correspondence: satchin@salk.edu
DOI 10.1016/j.cmet.2012.04.019

SUMMARY

While diet-induced obesity has been exclusively attributed to increased caloric intake from fat, animals fed a high-fat diet (HFD) ad libitum (ad lib) eat frequently throughout day and night, disrupting the normal feeding cycle. To test whether obesity and metabolic diseases result from HFD or disruption of metabolic cycles, we subjected mice to either ad lib or time-restricted feeding (tRF) of a HFD for 8 hr per day. Mice under tRF consume equivalent calories from HFD as those with ad lib access yet are protected against obesity, hyperinsulinemia, hepatic steatosis, and inflammation and have improved motor coordination. The tRF regimen improved CREB, mTOR, and AMPK pathway function and oscillations of the circadian clock and their target genes' expression. These changes in catabolic and anabolic pathways altered liver metabolome and improved nutrient utilization and energy expenditure. We demonstrate in mice that tRF regimen is a non-pharmacological strategy against obesity and associated diseases.

INTRODUCTION

In order to adapt to the daily cycles of nutrient availability, energy metabolism in animals has evolved to be cyclical. These metabolic cycles arise from cell-autonomous circadian rhythms and the feeding-fasting cycle, which drive genomic programs (Vollmers et al., 2009). At the molecular level, cell-autonomous circadian rhythms are based on interlocked negative feedback circuits in which BMAL1, CLOCK, NPAS2, and ROR proteins act as transcriptional activators and PER, CRY, and REV-ERB function as inhibitors to produce ~24 hr self-sustained rhythmic transcription of their own and target genes (reviewed in Reddy and O'Neill, 2010).

Feeding and fasting also drive daily rhythms in the activities of key regulators of nutrient homeostasis including AMPK, CREB, and AKT (Vollmers et al., 2009). There is extensive coupling between circadian oscillator components and the feeding-fasting-driven metabolic regulators. This coupling leads to coordinated oscillations at the transcript level and in the activities of a large number of neuroendocrine, signaling, and metabolic pathways that temporally link discordant cellular processes.

Perturbation of circadian oscillator components leads to obesity and diabetes, illustrating the importance of this interconnection. Genetic mouse models carrying either tissue-specific or whole-body loss-of-function or hypomorphic alleles of circadian oscillator components develop impaired glucose tolerance and signs of metabolic disease. Conversely, disruption of diurnal rhythms is commonly found in animal models of diabetes and obesity lacking specific metabolic regulators (reviewed in Bass and Takahashi, 2010). However, circadian oscillator components and metabolic regulators also control a large number of downstream effectors which do not exhibit any overt rhythms in expression (Cho et al., 2012; Feng et al., 2011; Rey et al., 2011). A number of mouse genetic models carrying whole-body- or tissue-specific perturbation of circadian oscillators (Cho et al., 2012; Kornmann et al., 2007; Lamia et al., 2008; Marcheva et al., 2010; Preitner et al., 2002; Turek et al., 2005) or key metabolic regulators (Andreelli et al., 2006; Herzig et al., 2001, 2003; Shaw et al., 2005) exhibit no profound defect in the overt rhythms in activity or feeding under normal light:dark cycle yet exhibit metabolic dysfunctions. Therefore, genetic models are inconclusive in addressing whether metabolic oscillations are necessary and sufficient for preventing metabolic diseases under nutritional challenge such as one posed by a high-fat diet (HFD).

To test whether robust metabolic cycles can protect against nutritional challenges that predispose to obesity, we adopted a widely used rodent model of diet-induced obesity. Mice fed a HFD ad libitum (ad lib) develop obesity, diabetes, and metabolic syndrome. However, they also exhibit dampened feeding and circadian rhythms (Kohsaka et al., 2007). Limiting access to HFD during day or night for up to 6 weeks shows some improvement in body weight regulation (Arble et al., 2009; Bray et al., 2010). However, since body weight and metabolic diseases are not always correlated (Ruderman et al., 1998; Wang et al., 2010), it is unclear whether time-restricted feeding (tRF) without changing caloric intake prevents metabolic diseases.

We subjected isogenic mice to either a diet of standard composition or one with high-fat content under two food-access paradigms: ad lib or time-restricted access for more than 100 days. tRF improved metabolic and physiologic rhythms, and protected the mice from the adverse effects of a HFD. The time-restricted high-fat-fed mice showed significantly increased thermogenesis and improved rhythms in nutrient utilization, leading to reduced adiposity and liver steatosis, normal glucose tolerance, reduced serum cholesterol, increased bile acid production, and improved motor function.

RESULTS

Time-Restricted Feeding Improves Overt Rhythms and Attenuates Body Weight Gain

To test whether a distinct tRF regimen can prevent diet-induced obesity, we subjected 12-week-old male C57BL/6J mice to HFD (61% energy from fat) or normal chow (NC; 13% fat) under either ad lib or time-restricted access to food during their natural nocturnal feeding time (Figure 1A). Mice fed NC under an ad lib regimen (NA) displayed diurnal rhythms in their food intake and whole-body respiratory exchange ratio (RER) (Figures 1B and 1C). Food intake and RER exhibited a nocturnal increase, reflective of feeding and subsequent carbohydrate utilization, and declined during the day, consistent with lipid oxidation during fasting. Mice fed a HFD under an ad lib regimen (FA) displayed dampened diurnal rhythms in food intake and RER. In contrast, mice fed NC or HFD under a tRF regimen (NT and FT) improved diurnal rhythms in their RER compared to their ad lib-fed counterparts, with higher RER during feeding and reduced RER during fasting, indicative of increased glycolysis and fat oxidation, respectively (Figure 1C). Although all four groups of mice showed overall comparable nocturnal activity, the mice on tRF regimen (NT and FT) showed increased activity and increased energy expenditure toward the end of the night (Figures 1D–1F). The average daily energy intake for individual mice in all four groups was equivalent throughout 18 weeks of the experiment (Figures 1G and 1H). When normalized for body weight, the mice on tRF paradigms, in fact, showed increased energy intake/unit body weight toward the end of the experiment (Figure 1I). Most remarkably, despite equivalent energy intake from the same nutrient source, FT mice were protected against excessive body weight gain that afflicted FA mice (Figures 1J and 1K and see Figure S1 online), suggesting that the temporal feeding pattern reprograms the molecular mechanisms of energy metabolism and body weight regulation.

Temporal Feeding Pattern Shapes Rhythms in CREB, mTOR, and AMPK Activities and in the Circadian Oscillator

A HFD fed under an ad lib regimen perturbs metabolic regulators, including CREB, mTOR, and AMPK, and contributes to metabolic diseases (Altarejos and Montminy, 2011; Inoki et al., 2011). Hepatic CREB phosphorylation is elevated during fasting, consistent with the role of active pCREB in gluconeogenesis (Herzig et al., 2001), while insulin and mTOR-stimulated pS6 levels (Um et al., 2006) are elevated during feeding. In NA mice, the diurnal rhythm in food intake (Figure 1B) induced hepatic CREB phosphorylation during daytime fasting and increased pS6 levels during nighttime feeding (Figures 2A and 2B). In FA mice, the perturbed circadian feeding pattern blunted pCREB and pS6 oscillations and led to constitutively elevated pCREB and reduced pS6 levels. In contrast, in the FT mice, the tRF imposed a diurnal rhythm in food intake, thereby restoring the daytime peak in pCREB and nighttime peak in pS6. The diurnal rhythm in food intake and associated daily fasting period under the FT paradigm increased the hepatic AMP levels relative to that seen in the FA paradigm (Figure 2C). Upon allosteric activation by AMP, AMPK, a master regulator of energy metabolism, phosphorylates and deactivates one of the rate-limiting enzymes of fatty acid oxidation, acetyl CoA carboxylase (ACC) (Davies et al., 1990). Thus, increased AMP and phospho-ACC (pACC, relative to total ACC) (Figures 2C and 2D, Figures S2A–S2C, and Table S1) in the livers of FT mice reflected increased AMPK activity relative to the livers of FA mice.

During fasting, AMPK phosphorylates a circadian repressor CRY (Lamia et al., 2009) and targets it for subsequent degradation, thus preventing it from repressing CLOCK:BMAL1 target genes, such as *Rev-erbα*, *Per*, and *Cry*. During feeding, mTOR activity indirectly modulates *Per* expression (Giebultowicz and Kapahi, 2010). Under the FA regimen, perturbed total and/or diurnal change in active CREB, mTOR, and AMPK reduced the mRNA levels and/or dampened the oscillations of circadian clock components (*Per1*, *Per2*, *Cry1*, *Bmal1*, *Clock*, *Rorα*, *Rev-erbα*, and an immediate output target, *Dbp*) in the liver (Figure 2E and Figure S2D). Under the FT regimen, the imposed feeding rhythms resulted in improved oscillations of circadian clock components in the liver, with an increase in the peak to trough ratio of mRNA levels. NA mice show a robust feeding rhythm and clear oscillations in clock gene expression, which is moderately improved by feeding consolidation in the NT mice.

Hepatic Glucose Metabolism Is Improved under Time-Restricted Feeding

Coordination among circadian oscillator components and metabolic regulators helps maintain glucose homeostasis and anabolic metabolism in the liver. Rhythmic *Cry* expression and pCREB oscillation synergistically suppress gluconeogenic gene expression (Vollmers et al., 2009; Zhang et al., 2010). Accordingly, in the livers of FT mice, improved CRY expression and suppressed nocturnal pCREB (Figures 2A and 2E) reduced the mRNA levels of gluconeogenic CREB target genes *Pyruvate carboxylase* (*Pcx*) and *Glucose-6-phosphatase* (*G6pc*) (Figures 3A and 3B), which encode enzymes that mediate the committing step in gluconeogenesis. With reduced *Pcx* and *G6pc* gene expression, pyruvate is likely used in the TCA cycle, since the levels of several TCA cycle intermediates (e.g., malate, fumarate, and citrate) are increased in the livers of FT mice (Figure 3C and Table S1). In parallel, reduced dephosphorylation of glucose-6-phosphate (G6-P) contributed to lowering blood glucose by decreasing the release of free glucose. The increased G6-P in the FT liver (Figure 3C) is likely diverted to the pentose phosphate cycle (PPC).

mTOR induces the expression of *glucose-6-phosphate dehydrogenase* (*G6pdx*) (Duvel et al., 2010), whose protein product is the rate-limiting enzyme of the PPC and is activated by accumulation of its substrate G6-P. In turn, the PPC is a major source of

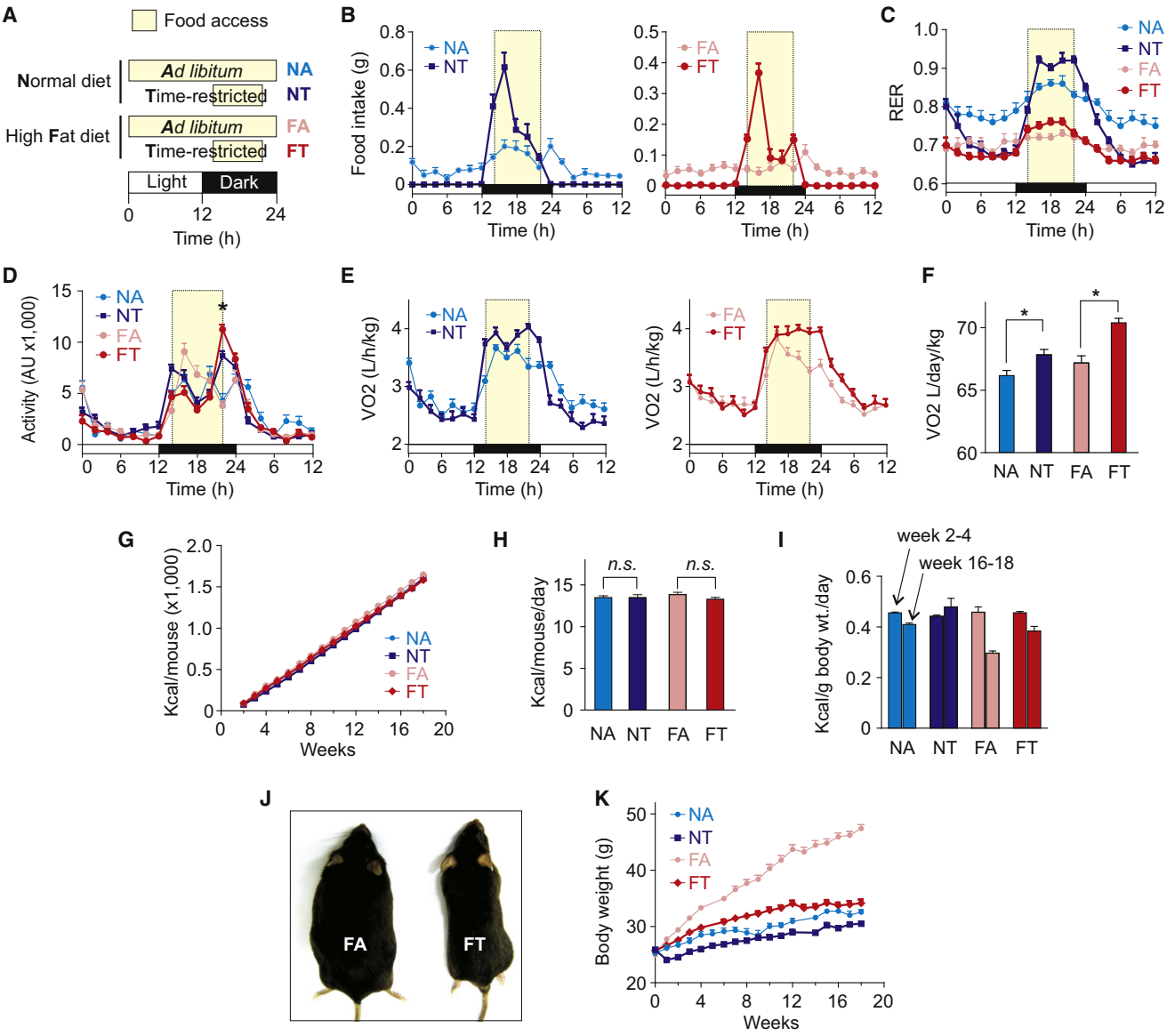

Figure 1. Time of Feeding Shapes Diurnal Pattern of Whole-Body Metabolism and Influences Body Weight Gain

(A) Schematic outline of the four feeding regimens used in this study. Time-restricted-fed mice were allowed access to food from ZT13 through ZT21. Food availability is indicated by light beige boxes.

(B–E) Shown are (B) food ingested, (C) respiratory exchange ratio (CO_2 exhaled/O_2 inhaled), (D) average activity, and (E) whole-body energy expenditure as measured by volume of O_2 consumed in 2 hr bins plotted against time (+SEM, n = 4 mice). Since the high-fat diet (HFD) is energy rich (5.51 Kcal/g), the mice on HFD consume an amount of energy equivalent to that of the mice on normal chow (NC) (3.36 Kcal/g).

(F) Area under the curve analyses of energy expenditure (from Figure 1E) (+SEM, n = 4, *p < 0.05). Given the differences in body composition, metabolic activities in different organs, and heterogeneity of substrate uses in different groups of mice, both food intake and energy expenditures were expressed relative to individual animal or unit body weight.

(G and H) (G) Cumulative average energy intake or (H) average daily energy intake (+SEM, n = 24 over 17 weeks) by individual mice on NC or HFD is not significantly different (n.s., p > 0.05) under ad lib or tRF paradigm. The near-equivalent average energy intake from NC and HFD is not different from several published studies. Voluntary energy intake is often independent of dietary fat content both in rodents and in human twins (examples include but are not limited to Bray et al., 2010; Fujisaka et al., 2011; Hosooka et al., 2008; Kennedy et al., 2007; Lin et al., 2000; Saltzman et al., 1997; Samuel et al., 2004), and these studies also show that irrespective of caloric intake, voluntary ingestion of HFD predisposes to obesity, diabetes, and related diseases. The higher proportion of energy intake from fat is usually considered the cause for diet-induced obesity in these studies.

(I) Average energy intake (+SEM) normalized to unit body weight shows no difference at the beginning of the experiment. In the subsequent weeks with gradual increase in body weight, this value progressively declines. By the end of 16–18 weeks, mice on tRF consume more energy/unit body weight than the ad lib counterparts.

(J) Representative FT mouse was remarkably leaner than the FA mouse.

(K) Average body weight (+SEM, n = 20–32 mice). Also see Figure S1.

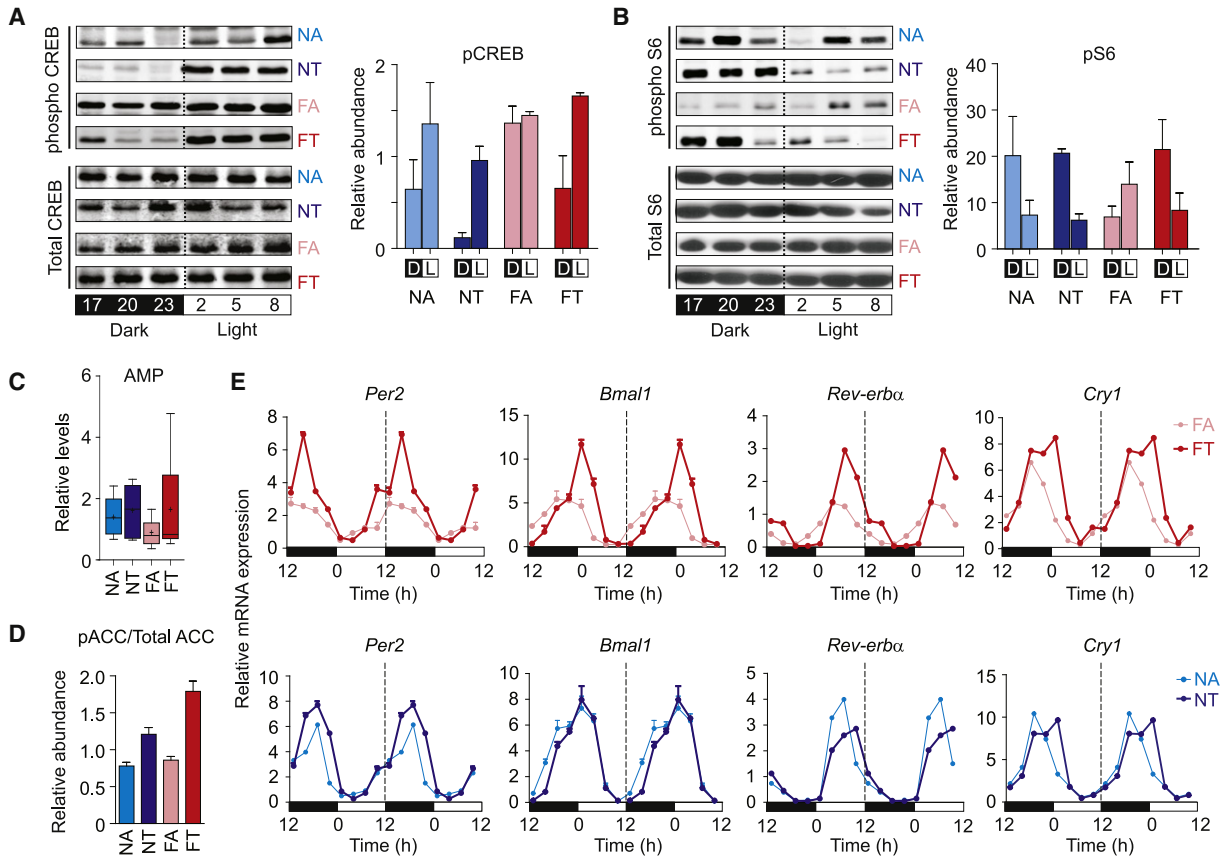

Figure 2. Time-Restricted Feeding Improves Diurnal Rhythms in Metabolic Regulators and the Circadian Oscillator

(A and B) Representative immunoblots and densitometry quantification of the immunoblots (average [+SEM, n = 3] during feeding and fasting in the tRF mice, which coincide with night and day, respectively) for (A) transcriptionally active phospho-Ser133-CREB (pCREB) and (B) phospho-S6 (pS6) in the mouse liver.

(C) Whisker plot showing the AMP level in the liver of FT mice is significantly higher than that in FA mice. Error bars denote maximum and minimum of distribution.

(D) Proportion of phospho-ACC (pACC) relative to total ACC from mouse liver (also see Figure S2).

(E) Double-plotted average (+SEM, n = 4) mRNA levels of circadian oscillator components *Per2*, *Bmal1*, *Rev-erbα*, *Cry1*, and additional clock components (Figure S2D) in liver at different times of the day. Transcript levels were measured by qRT-PCR and normalized to *Gapdh* mRNA levels. Broken line separates double plotted data. Also see Figure S2.

NADPH, which reduces glutathione. In the livers of mice under tRF, induced expression of *G6pdx* along with elevated G6-P led to increased activity of the PPC as measured by higher levels of PPC intermediates and of reduced glutathione (Figures 3D and 3E and Figure S3).

The pentose sugars of PPC and intermediates of TCA cycle are substrates for both de novo and salvage pathways of nucleotide biosynthesis. Several genes encoding enzymes of purine and pyrimidine biosynthesis and nucleotide salvage pathways are the direct targets of the circadian activator BMAL1 (*Uridine monophosphate synthase* [*Umps*] and *Thymidine kinase 1* [*Tk1*]) and/or exhibit rhythmic expression patterns (*phosphoribosylpyrophosphate synthetase* [*Prps-1,-2*], *phosphoribosyl pyrophosphate amidotransferase* [*Ppat*] and *Carbamoyl phosphate synthetase/aspartate transcarbamylase/dihydroorotase* [*Cad*]) (Hughes et al., 2009; Nakahata et al., 2009; Ramsey et al., 2009; Rey et al., 2011; Vollmers et al., 2009). In the FT livers, increased *Bmal1* mRNA led to a parallel increase in the mRNA levels of *Umps* and *Tk1* as well as elevated levels of both purine and pyrimidine metabolites (Figures 3F–3H, Figures S3 and S4A). These coordinated changes in gene expression and metabolites show that the tRF regimen temporally reprograms glucose metabolism away from gluconeogenesis toward glycolysis, reduced glutathione, and anabolic pathways. Accordingly, FT mice did not display the hallmarks associated with glucose intolerance found in diet-induced obesity, instead showing glucose tolerance and insulin levels comparable to the control NA mice (Figures 3I and 3J). The overall improvement in metabolic state also paralleled improved motor coordination in the mice under tRF paradigms (Figure 3K).

The Temporal Pattern of Feeding Determines Lipid Homeostasis

The circadian oscillator components interact with metabolic regulators to maintain lipid homeostasis. In the livers of FT mice, increased levels of the transcriptional repressor *Rev-erbα* (Figure 2E) led to reduced expression of its direct target and a key lipogenic gene, fatty acid synthase (*Fasn*) (Cho et al.,

2012) (Figure 4A). Reduced *Fasn* mRNA levels (Figure 4A) and increased relative pACC levels (Figure 2D) are known to contribute to a decline in the level of several long-chain free fatty acids (Harwood, 2004), including myristate and palmitate (Figure 4B and Table S1). In parallel, increased *Per2* expression in FT liver (Figure 2E) acts as an inhibitor of already-reduced levels

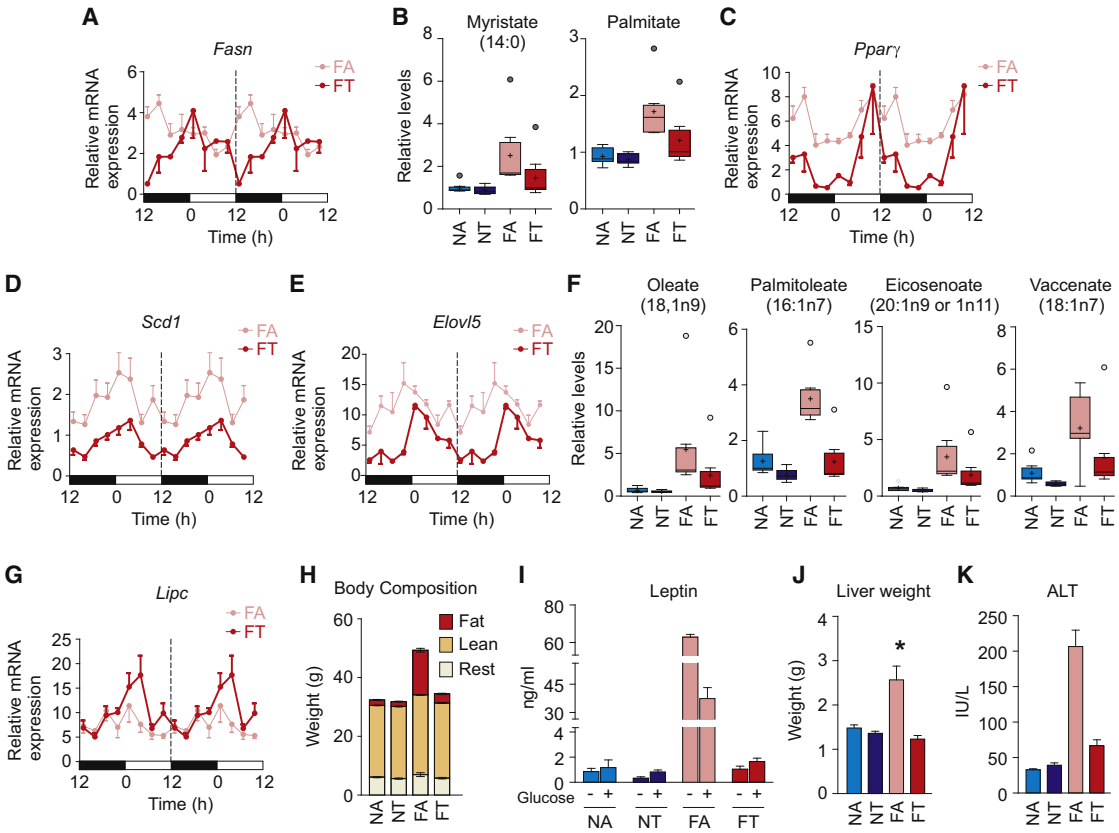

Figure 4. Time-Restricted Feeding Alters Fatty Acid Metabolism and Prevents Obesity and Liver Pathology

(A and B) (A) Reduced hepatic mRNA levels of REV-ERBα target gene *Fasn* in the livers of FT mice contribute to (B) the reduction in free fatty acids myristate and palmitate.

(C–G) Reduced mRNA levels of (C) *Pparγ*, (D) *Scd1*, and (E) *Elovl5* in the liver of FT mice (also see Figure S3) accompanied reduced levels of several unsaturated fatty acids including (F) oleate, palmitoleate, eicosenoate, and vaccinate (also see Figure S4B). Reduced malonyl-carnitine, increased BHBA (see also Figure S4B), and (G) increased *Lipc* mRNA are indicative of increased β-oxidation.

(H) Body composition analyses by MRI illustrate that tRF prevents excessive whole-body fat accumulation in mice fed HF diet. Average weights of fat, lean, and remaining body mass are shown.

(I) Increased levels of leptin after overnight fasting (−) and after glucose administration (+) indicative of increased adipose tissue in FA mice are absent in the FT mice.

(J and K) (J) tRF also prevents enlarged liver and (K) liver damage assessed by increased serum ALT.

In (B) and (F), error bars denote maximum and minimum of distribution with extreme data points marked (o).

of *Pparγ* (Figure 4C) (Grimaldi et al., 2010), further attenuating PPARγ-driven lipogenic gene expression. Repression of the PPARγ target gene *Stearoyl coA desaturase1* (*Scd1*) (Figure 4D), which encodes an enzyme mediating fatty acid desaturation, along with the reduced mRNA levels of the unsaturated fatty acid elongase *Elovl5* (Figure 4E and Figure S3) coincides with >50% decline in several unsaturated fatty acids, including oleate (18:1n9), palmitoleate (16:1n7), vaccenate (18:1n7), and eicosenoate (20:1n9 or 11) (Figure 4F and Figure S4B). Altogether, we observed reduced fatty acid synthesis, elongation, and desaturation in the livers of FT mice compared to those of the FA mice.

Fatty acid synthesis inhibits mitochondrial β-oxidation. Malonyl-CoA, a product of ACC activity in the first step of fatty acid synthesis, allosterically inhibits mitochondrial carnitine palmitoyltransferase (CPT). CPT is essential for the transit of long-chain fatty acids and acylcarnitine esters into the mitochondria for β-oxidation. Increased hepatic malonylcarnitine levels in FA mice, but not in FT mice (Figure S4B), are indicative of the specific disruption of fatty acid oxidation caused by impaired entry of fatty acids into the mitochondria. Conversely, increased hepatic lipase (*Lipc*) expression (Figure 4G) along with 3-hydroxybutyrate (BHBA) (Figure S4B), one of the end products of β-oxidation, in FT mice relative to FA mice indicated that tRF enhanced lipolysis and β-oxidation, further contributing to reduction in liver free fatty acids.

Time-Restricted Feeding Prevents Excessive Body Weight Gain, Hepatosteatosis, and Liver Damage

Among mice fed NC, the tRF regimen resulted in moderately lower weight (NT, 30.5 ± 0.4 g; mean ± SEM, n = 24) than the ad lib regimen (NA, 32.6 ± 0.4 g) (Figure 1K). In contrast, tRF remarkably reduced obesity in mice fed a HFD. Mice with ad lib access to HFD (FA) attained an average body weight of 47.4 g ± 0.7 g by 18 weeks in the feeding regimen (Figure 1K),

while FT mice weighed 28% less (34.2 ± 0.6 g) and were comparable to the NA group. Most of the extra body weight in the FA mice was due to increased adiposity (Figure 4H). FA mice showed 70% more fat deposits than those in the FT mice (FA 18.0 ± 1.03 g and FT 4.3 ± 1.23 g, $p < 0.05$). Consequently, hyperleptinemia associated with diet-induced obesity in FA mice was absent in FT mice (Figure 4I).

FT mice were also protected from the hepatomegaly and elevated serum alanine aminotransferase (ALT) levels that are associated with obesity-induced hepatic steatosis (Figures 4J and 4K). To further characterize the pathologic state and steatosis of the liver in these four groups, we used a Brunting scoring system under blinded conditions. Tissue samples from the FT mice had significantly less hepatic steatosis compared to those from the FA mice (Figures 5A and 5B). In addition, volume analyses of serial block-face scanning electron microscope images of the liver samples revealed that livers from the FT mice did not have the profound increase in intracellular fat deposits, reduced mitochondrial density, and reduced endoplasmic reticulum that were characteristic of the liver samples from the FA mice (Figures 5C and 5D and Table S2).

The liver disease in FA mice was associated with an increase in markers of inflammation. The increased pool of free fatty acids in the livers of FA mice included proinflammatory long-chain n-6 fatty acids dihomo-linoleate (20:2n6) and arachidonate (20:4n6) (Figure S4C). Oxidation of arachidonate and linoleic acid in an oxidative environment marked by decreased glutathione in the livers of the FA mice further increased the levels of proinflammatory eicosanoids: 15-hydroxyeicosatetraenoic acid (HETE), 5-HETE, and 13-HODE. In contrast, the suppressed lipogenic program along with a glutathione-enriched cellular environment in the livers of the FT mice attenuated the levels of proinflammatory lipids (Figure S4C).

Additional gene expression signatures often associated with hepatic inflammation and fatty liver disease (Figure 5E and Figure S5) were either reversed or attenuated under a tRF regimen. Changes in hepatic expression of nuclear hormone receptors *Rarα*, *Rxrα*, *Lxrα*, and *Lxrβ*, a characteristic of diet-induced obesity (Kohsaka et al., 2007), are prevented upon tRF. Increased expression of several genes encoding key enzymes for lipid metabolism, including *Crat* (cytoplasmic carnitine acyltransferase), *Me1* (malic enzyme producing reducing NADPH for fat synthesis), and *Mogat1* (monoacylglycerol O-acyltransferase 1) in the FA mice return to NC-fed levels in the FT group. Similarly, higher expression of lipid droplet-associated and lipolysis inhibitor gene *Cidec* (Puri et al., 2007), triglyceride storage-associated protein *CD36* (Koonen et al., 2007), and plasma triglyceride marker *ApoA4* (Talmud et al., 2002) in the liver of FA mice are reduced in the FT mice. The expression of *Cdkn1a* (*p21*), a cell cycle regulator, and of *Lgals1* (*Galectin-1*), a hepatocellular carcinoma and metastasis marker (Camby et al., 2006), is elevated in the FA group and reduced under tRF. High-fat ad lib feeding (FA) reduced expression of antidiabetic gene *Igfbp2* (Hedbacker et al., 2010), while tRF elevated expression irrespective of the nutrient source. Additionally, *Fabp1* (Fatty acid binding protein 1), which binds to and clears potentially toxic unesterified long-chain fatty acids from the cytoplasm (Atshaves et al., 2010), exhibits a moderate increase in expression in the liver of FT mice.

Time-Restricted Feeding Raises Bile Acid Production, Improves Adipose Tissue Homeostasis, and Alleviates Inflammation

Hepatic fatty acid metabolism contributes to cholesterol and bile acid homeostasis. Both the diurnal rhythms in food intake and the clock component *Rev-erbα* are known to participate in the diurnal production of cholesterol and bile acids through transcriptional regulation of the lipid homeostasis regulator *Srebp1c* and several rate-limiting enzymes including *Hmgcs2* and *Cyp7a1* (Cho et al., 2012; Le Martelot et al., 2009). Distinct feeding rhythms along with improved *Rev-erbα* rhythms in the livers of the FT regimen mice altered expression of *Srebp1c*, *Hmgcs2*, and *Cyp7a1* (Figures 6A and 6B, Figures S3 and S5). Increased peak levels of *Cyp7a1* mRNA, which encodes the rate-limiting step in bile acid production from cholesterol, elevated hepatic bile acids and contributed to a decrease in serum cholesterol levels in the FT mice (Figures 6C and 6D, Figure S6, and Table S1). Although the liver is efficient in reabsorbing bile acids, increased postprandial hepatic bile acids spill over into circulation and raise energy expenditure in brown adipose tissue (BAT) by inducing expression of the uncoupling proteins (Watanabe et al., 2006). Indeed, in BAT derived from FT mice, we observed increased and rhythmic *UCP* expression (Figure 6E) which paralleled nighttime energy expenditure as measured by whole-body oxygen use (Figures 1E and 1F), as well as improved circadian oscillator function and increased *PPARα* expression (Figure 6E).

Elevated β-oxidation and reduced fatty acid synthesis in the liver coupled with increased BAT energy expenditure observed in the FT mice prevented the adipocyte hypertrophy common to BAT and white adipose tissue (WAT) derived from the FA mice (Figures 6F and 6G). Furthermore, inflammation marked by extensive infiltration of macrophages and expression of proinflammatory genes including *TNFα*, *IL6*, and *CXCL2* that are generally found in the WAT of the FA mice, were attenuated in the FT mice (Figure 6H). Even in mice fed a normal diet, tRF reduced the expression of inflammatory cytokines in the WAT. In summary, the tRF paradigm affected multiple tissues, improved whole-body energy homeostasis, and reduced inflammation.

DISCUSSION

Obesity is a major health challenge in many developed countries, reaching global pandemic proportions (Finucane et al., 2011). The prevalence of obesity has risen unabated for the last four decades, currently affecting 35.5% of the population of United States and projected to affect as much as 50% of the population in another four decades (King, 2011). The morbidity and mortality of its associated metabolic diseases, as well as its economic impact (Hammond and Levine, 2010), has made finding treatments for obesity an imperative of multiple national health agencies. Lifestyle modification is the first-line intervention in the treatment of obesity due to ease of access and lower cost over pharmacotherapy or surgery (McTigue et al., 2003). The focus of currently recommended lifestyle modification has been altering nutrition. In a murine model, here we introduce a lifestyle intervention that can prevent obesity as well as its associated metabolic disorders by preserving natural feeding rhythms without altering nutrition intake.

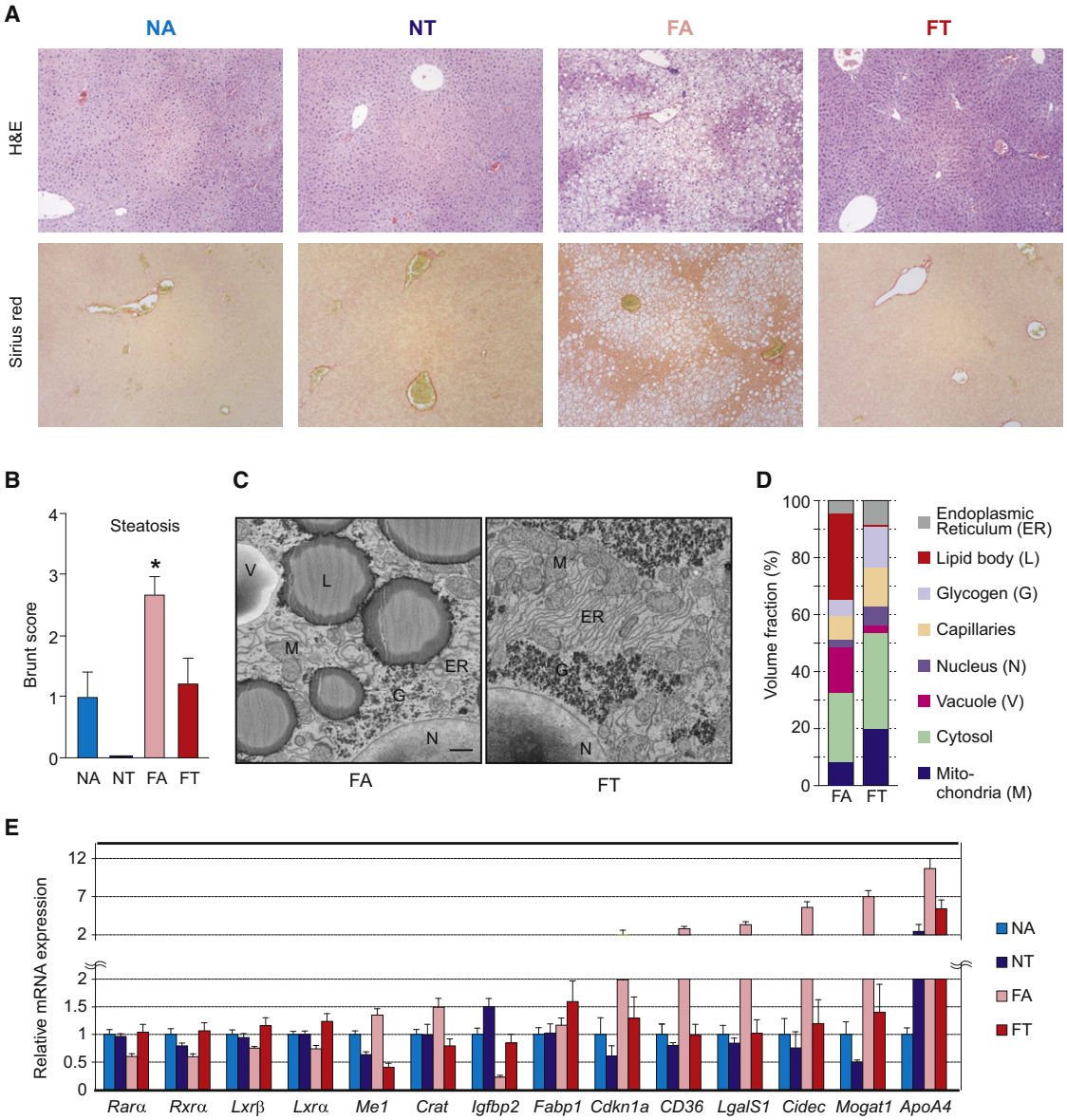

Figure 5. Time-Restricted Feeding Prevents Liver Diseases

(A) Representative histology (upper panel, H&E, scale bars, 200 μm; and lower panel, Sirius red, scale bars, 200 μm) of the liver. Steatohepatitis was scored by a histopathologist who was blinded to the source condition of each sample using a semiquantitative method derived from Brunt et al. (Brunt et al., 2004) measuring the degree of steatosis (0–3), ballooning degeneration (0–2), lobular (0–3) and portal (0–2) inflammation, and fibrosis (0–4).

(B) Average steatosis score (+SEM, n = 4 mice) of liver sections.

(C) Representative scanning electron microscope image of a liver from FA mice shows large lipid droplets and vacuoles that are reduced in FT liver. Scale bar, 1 μm.

(D) Measurement of several volume fractions shows FT regimen prevents the decline in density of mitochondria and ER under *ad lib* HF diet (FA). Measurements are from a volume rendering obtained from serial block-face images of the liver. See also Table S2.

(E) Gene expression signature of diet-induced obesity in the mouse liver is attenuated by tRF. Average expression (+SEM) from eight different time points (Figure S2A) are shown in bar graphs. Significant differences between FA and FT ($p < 0.05$) were found. Temporal expression profiles of these genes are shown in Figure S5.

Although it has long been assumed that the cause of adiposity associated with mouse models of diet-induced obesity is nutritional, there is an emerging suggestion that the temporal spreading of calorie intake could be contributing as well. Under ad lib access to food, a HFD blunts the diurnal feeding rhythms more severely than a standard diet (Figure 1B). Therefore, mice fed HFD ad lib have a short fasting period and a long feeding window. This feeding pattern perturbs metabolic pathways entrained by both circadian and feeding rhythms. The temporal disruption in cellular metabolic processes, in combination with the nutrient quality, predisposes the organism to obesity and metabolic diseases.

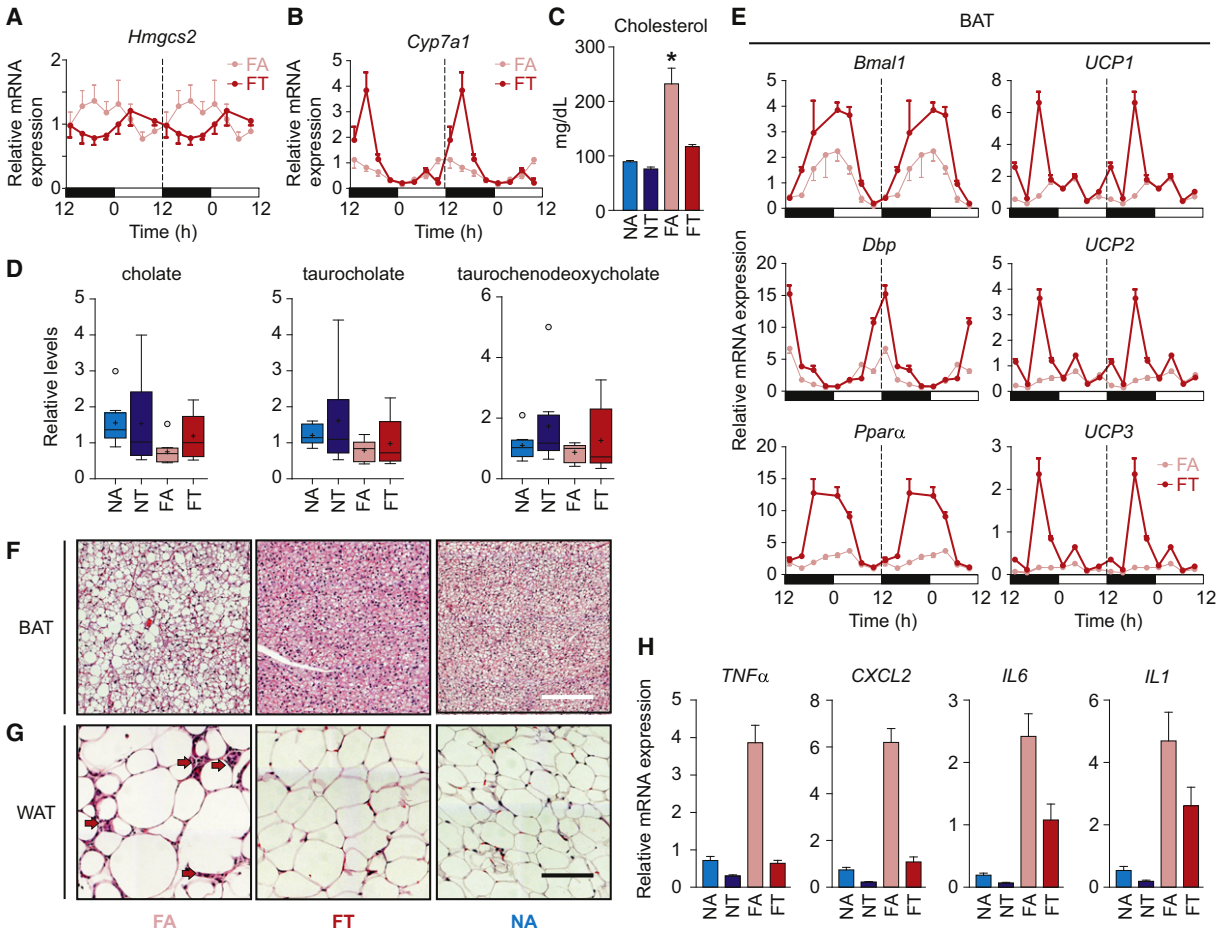

Figure 6. Time-Restricted Feeding Modulates Bile Acid Metabolism, Energy Expenditure, and Inflammation

(A–D) tRF regimen (A) suppressed the expression of *Hmgcs2* and (B) increased the expression of *Cyp7a1* in the liver, which accompanied (C) a reduction in serum cholesterol and (D) an increase in hepatic bile acids. Relative levels of representative bile acids are shown (also see Figure S6). Error bars denote maximum and minimum of distribution with extreme data points marked (o).

(E–H) (E) qRT-PCR measurements of relative mRNA levels of *Bmal1*, *Dbp*, and *Pparα* show robust circadian oscillation in the BAT of FT mice (also see Figure S3 for NA and NT gene expression). Increased expression of *UCP1-3* during the late night correlates with increased energy expenditure in FT mice (Figure 1). H&E-stained sections of (F) BAT or (G) WAT show that the adipocyte hypertrophy seen in FA mice is prevented in the FT mice. Scale bar, 50 μm. Arrows indicate infiltrating cells that are most likely macrophages. Reduction in infiltrating macrophages also correlates with a reduction in (H) the mRNA levels of several proinflammatory cytokines in the WAT of FT mice. Average (+SEM, n = 8) mRNA levels of proinflammatory cytokines *TNFα*, *CXCL2*, *IL6*, and *IL1* in the WAT are reduced under the tRF paradigm.

The tRF regimen entrained the circadian clock and metabolic regulators to fixed feeding times and prevented high-fat-diet-induced disruption of the normal cellular metabolic program. Compared to their NC counterparts, the beneficial effect of tRF on the gene expression (Figures 2–6, Figures S3 and S5) and metabolic signatures is more pronounced in mice fed a HFD. Liver metabolome analyses detected 324 named metabolites common to all four groups of mice, of which 240 (74%) changed between at least one pair of feeding regimen (Figures 7A and 7B, Table S1, and http://metabolites.salk.edu/), thus highlighting that both nutrient quality and the daily feeding pattern are important determinants of the liver metabolic homeostasis. Among mice fed a standard diet, time of food access changed the overall levels of 56 metabolites, while 123 metabolites changed between mice under FA and FT regimen. Both the average levels and diurnal oscillations of these metabolites are defined by the time of feeding (Figures 7C–7E and Figure S7).

Implicit in our findings is that the control of energy metabolism is a finely tuned process that involves an intricate network of signaling pathways and transcriptional effectors, including nutrient-sensing mechanisms and the circadian system. tRF acted on these interwoven networks and moved their state toward that of a normal feeding rhythm. In addition to nutrient metabolism, pathways regulating steady-state levels of signaling molecules and cofactors in the liver such as bile acids, sterols, riboflavin, heme, and coenzyme-A (Figure 7E, Figure S7, and Table S1) are also affected by the time of feeding. These signaling molecules and cofactors likely affect functions of multiple other organs, partly explaining how feeding rhythms can indirectly have systemic consequences. The beneficial

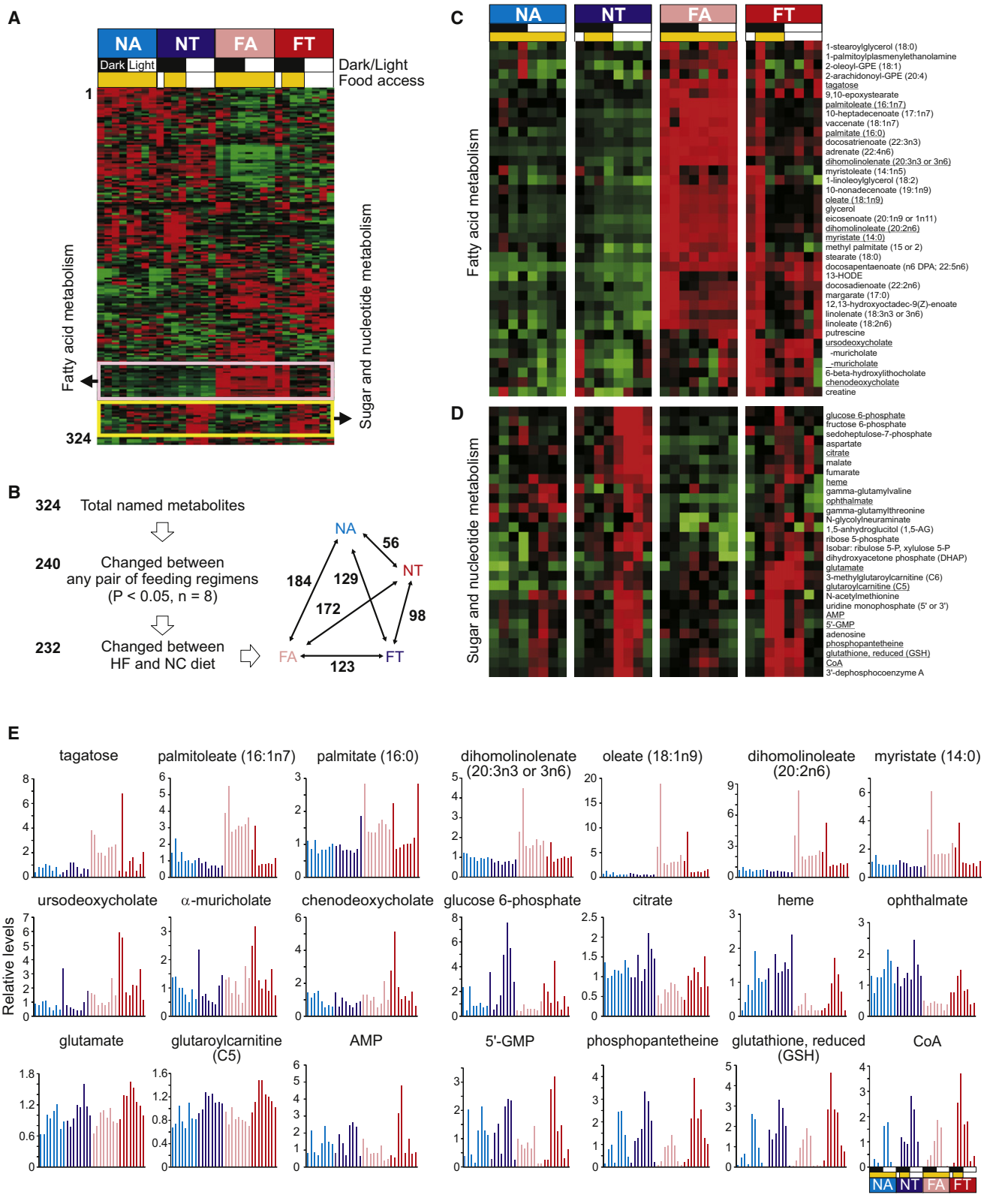

Figure 7. Time of Feeding Exerts a Profound Effect on Liver Metabolites in Mice on a High-Fat Diet

(A) Heatmap rendering of normalized levels of 324 liver metabolites at eight different time points in the liver of NA, NT, FA, and FT groups of mice. The metabolites were clustered by hierarchical clustering.

effects of tRF were also evident in mice fed NC, implying that tRF might improve metabolism under diverse nutritional challenges.

Although a number of clinical studies have shown that the perturbation of light:dark or sleep:wake cycle (e.g., shiftwork) has adverse metabolic consequences in humans, there is very little information on the perturbation of eating rhythms in the participants of these studies. Hence, the contribution of frequent feeding and reduced daily fasting period to obesity, type 2 diabetes, and other adult-onset metabolic diseases is unclear. Current public health surveys on human nutrition focus on the quality of nutrition and quantity of food consumption with no evidence-based method in place to monitor temporal pattern of food intake. More studies are necessary to define the relationship between temporal eating and obesity in humans. The results presented in our study with mice suggest that tRF could be a nonpharmacological intervention in humans that could prevent obesity and its associated metabolic disorders.

EXPERIMENTAL PROCEDURES

Animals

All animal experiments were carried out in accordance with the guidelines of the Institutional Animal Care and Use Committee of the Salk Institute. The feeding regimen experiments were repeated on four independent batches of mice, and representative data sets are presented here. Whole-body indirect calorimetry was carried out on a subset of mice at 4, 8, or 12 weeks, and all other measurements were carried out on a subset of mice at least 12 weeks after the initiation of the feeding regimens.

Feeding Schedule and Diets

Eight-week-old male C57BL/6J mice from Jackson Laboratory were group housed (three to five mice per cage) under a 12 hr light:12 hr dark schedule for 4 weeks to adapt to the housing condition. They were fed NC (LabDiet 5001; 29% protein, 13% fat, 58% carbohydrates) or HFD (LabDiet 58Y1; 18% protein, 61% fat, 21% carbohydrates) either with unrestricted (ad lib) or temporally restricted access to food (tRF) (see Figure 1A). Under tRF, mice were allowed access to food between ZT13 (1 hr after lights off) and ZT21 (3 hr before lights on). Food access was regulated by transferring mice daily between cages with food and water and cages with water only. To control for mouse handling, ad lib-fed mice were also transferred between feeding cages at the same time. Weekly food intake was measured by monitoring the weight of the remaining food.

Metabolic Cages

Whole-body metabolic states were tested by indirect calorimetry in a CLAMS system (Columbus Instruments) for 2 days after 4 days of habituation following the manufacturer's instructions. Light and feeding conditions were kept the same as in the home cages.

Glucose Tolerance

Mice were fasted for 16 hr, and fasted glucose was measured using a Glucometer (One Touch Ultra) by tail bleeds. Subsequently, mice were intraperitoneally injected with 1 g glucose/kg of body weight, and blood glucose was measured in intervals of 30 min for 2 hr.

Insulin and Leptin ELISAs

Overnight fasted mice were intraperitoneally injected with 1 g of glucose per kilogram of body weight, and retro-orbital blood was collected after 1 hr. Insulin (Crystal Chem #90080) and leptin (Millipore) ELISAs were measured in the blood of fasted and glucose-injected mice following manufacturer's instructions.

ALT and Cholesterol

Mice were fasted for 16 hr starting from ZT21, and blood was collected retro-orbitally. ALT and cholesterol were assayed by IDEXX Laboratories.

Rotarod

Mice were placed on accelerating (10—70 rpm) rotarods for up to 180 s. Mice were tested on two subsequent days. On the first day, the mice were given five trial runs for habituation. Data were collected from three runs on the second day after two trials runs.

Histology and Electron Microscopy

Sections (6 μm) of formaldehyde-fixed liver, WAT, and BAT were stained with H&E. Liver sections were also stained using Sirius red method. See the Supplemental Information for details.

Body Composition

Body fat and lean mass of live mice were assessed using a mouse MRI (Echo Medical Systems) following manufacturer's protocol.

Transcript, Protein, and Metabolite Analyses

Three to four mice in each feeding group were sacrificed every 3 hr over a 24 hr period, and individual liver, WAT, and BAT samples were flash frozen. Aliquots of frozen tissues were used for immunoblot and qRT-PCR analyses carried out as described earlier (Vollmers et al., 2009). Frozen liver aliquots were analyzed for detection and relative quantification of metabolites by Metabolon following published methods (Evans et al., 2009).

Statistical Tests

To account for diurnal variations in liver metabolites, samples collected at eight different time points throughout the day were analyzed and treated as replicates in ANOVA tests. For a given metabolite, the measured levels across all samples were median normalized to 1, and missing data points (if any) were imputed with the minimum values. Results were plotted in whisker plots where the box denotes the middle 80 percentile with mean (+) and median (–). Error bars denote maximum and minimum of distribution with extreme data points marked (o). The relative levels of all detected metabolites, changes in different feeding groups, and the associated statistical test results are presented in Table S1. Metabolic cage data, body weight, food consumed, and qRT-PCR results were analyzed by Student's t test (one tailed or two tailed based on sample types). Only in cases where the average values appear close, significant differences at $p < 0.05$ are denoted with "*." Average (+SEM) values are shown in the figures.

SUPPLEMENTAL INFORMATION

Supplemental Information includes seven figures, two tables, Supplemental Experimental Procedures, and Supplemental References and can be found with this article at doi:10.1016/j.cmet.2012.04.019.

(B) A summary of metabolite changes in the liver highlights the larger effect of temporal feeding pattern when animals were fed HFD. For statistical analyses, all eight time points for each feeding regimen were treated as replicates. Number of metabolites that changed between any two of the six different contrasts is shown in the right panel.

(C–E) (C) Heatmap rendering of a subset of metabolites of a cluster enriched for fatty acids and (D) another cluster enriched for intermediates of energy and anabolic metabolism. Tissues were harvested at ZT14, ZT17, ZT20, ZT23, ZT2, ZT5, ZT8, and ZT11. The time of food access is indicated in yellow boxes. Red, high; green, low. Steady-state levels of several of the metabolites at eight different time points representing one full day from (C) and (D) marked with underlined text are shown in (E). Normalized values presented in Table S1 are plotted against time.

ACKNOWLEDGMENTS

We thank Drs. Marc Montminy and Ron Evans for helpful comments and advice on the work and for sharing their research equipment. We also thank Hiep Le, Sheena Keding, Chrissta Maracle, and Ishika Arora for technical support. The IMOD stereology plug-in was developed by Andrew Noske, and we thank him for providing instruction and guidance. This work was partially supported by the Pew Scholars Program in Biomedical Sciences, NIH grant DK091618, Sanofi Discovery Innovation Grant, and The Anderson Foundation support to S.P.; The Japan Society for the Promotion of Science (JSPS) Fellowship to M.H.; The Blasker-Rose-Miah Fund of The San Diego Foundation to C.V.; NIH T32 DK07202 training grant to A.Z.; and NCRR grant 5P41RR004050 to M.H.E.

Received: February 7, 2012
Revised: March 18, 2012
Accepted: April 25, 2012
Published online: May 17, 2012

REFERENCES

Altarejos, J.Y., and Montminy, M. (2011). CREB and the CRTC co-activators: sensors for hormonal and metabolic signals. Nat. Rev. Mol. Cell Biol. *12*, 141–151.

Andreelli, F., Foretz, M., Knauf, C., Cani, P.D., Perrin, C., Iglesias, M.A., Pillot, B., Bado, A., Tronche, F., Mithieux, G., et al. (2006). Liver adenosine monophosphate-activated kinase-alpha2 catalytic subunit is a key target for the control of hepatic glucose production by adiponectin and leptin but not insulin. Endocrinology *147*, 2432–2441.

Arble, D.M., Bass, J., Laposky, A.D., Vitaterna, M.H., and Turek, F.W. (2009). Circadian timing of food intake contributes to weight gain. Obesity (Silver Spring) *17*, 2100–2102.

Atshaves, B.P., Martin, G.G., Hostetler, H.A., McIntosh, A.L., Kier, A.B., and Schroeder, F. (2010). Liver fatty acid-binding protein and obesity. J. Nutr. Biochem. *21*, 1015–1032.

Bass, J., and Takahashi, J.S. (2010). Circadian integration of metabolism and energetics. Science *330*, 1349–1354.

Bray, M.S., Tsai, J.Y., Villegas-Montoya, C., Boland, B.B., Blasier, Z., Egbejimi, O., Kueht, M., and Young, M.E. (2010). Time-of-day-dependent dietary fat consumption influences multiple cardiometabolic syndrome parameters in mice. Int. J. Obes. (Lond.) *34*, 1589–1598.

Brunt, E.M., Neuschwander-Tetri, B.A., Oliver, D., Wehmeier, K.R., and Bacon, B.R. (2004). Nonalcoholic steatohepatitis: histologic features and clinical correlations with 30 blinded biopsy specimens. Hum. Pathol. *35*, 1070–1082.

Camby, I., Le Mercier, M., Lefranc, F., and Kiss, R. (2006). Galectin-1: a small protein with major functions. Glycobiology *16*, 137R–157R.

Cho, H., Zhao, X., Hatori, M., Yu, R.T., Barish, G.D., Lam, M.T., Chong, L.W., Ditacchio, L., Atkins, A.R., Glass, C.K., et al. (2012). Regulation of circadian behaviour and metabolism by REV-ERB-alpha and REV-ERB-beta. Nature *485*, 123–127.

Davies, S.P., Sim, A.T., and Hardie, D.G. (1990). Location and function of three sites phosphorylated on rat acetyl-CoA carboxylase by the AMP-activated protein kinase. Eur. J. Biochem. *187*, 183–190.

Duvel, K., Yecies, J.L., Menon, S., Raman, P., Lipovsky, A.I., Souza, A.L., Triantafellow, E., Ma, Q., Gorski, R., Cleaver, S., et al. (2010). Activation of a metabolic gene regulatory network downstream of mTOR complex 1. Mol. Cell *39*, 171–183.

Evans, A.M., DeHaven, C.D., Barrett, T., Mitchell, M., and Milgram, E. (2009). Integrated, nontargeted ultrahigh performance liquid chromatography/electrospray ionization tandem mass spectrometry platform for the identification and relative quantification of the small-molecule complement of biological systems. Anal. Chem. *81*, 6656–6667.

Feng, D., Liu, T., Sun, Z., Bugge, A., Mullican, S.E., Alenghat, T., Liu, X.S., and Lazar, M.A. (2011). A circadian rhythm orchestrated by histone deacetylase 3 controls hepatic lipid metabolism. Science *331*, 1315–1319.

Finucane, M.M., Stevens, G.A., Cowan, M.J., Danaei, G., Lin, J.K., Paciorek, C.J., Singh, G.M., Gutierrez, H.R., Lu, Y., Bahalim, A.N., et al. (2011). National, regional, and global trends in body-mass index since 1980: systematic analysis of health examination surveys and epidemiological studies with 960 country-years and 9.1 million participants. Lancet *377*, 557–567.

Fujisaka, S., Usui, I., Kanatani, Y., Ikutani, M., Takasaki, I., Tsuneyama, K., Tabuchi, Y., Bukhari, A., Yamazaki, Y., Suzuki, H., et al. (2011). Telmisartan improves insulin resistance and modulates adipose tissue macrophage polarization in high-fat-fed mice. Endocrinology *152*, 1789–1799.

Giebultowicz, J., and Kapahi, P. (2010). Circadian clocks and metabolism: the nutrient-sensing AKT and TOR pathways make the link. Curr. Biol. *20*, R608–R609.

Grimaldi, B., Bellet, M.M., Katada, S., Astarita, G., Hirayama, J., Amin, R.H., Granneman, J.G., Piomelli, D., Leff, T., and Sassone-Corsi, P. (2010). PER2 controls lipid metabolism by direct regulation of PPARgamma. Cell Metab. *12*, 509–520.

Hammond, R.A., and Levine, R. (2010). The economic impact of obesity in the United States. Diabetes Metab. Syndr. Obes. *3*, 285–295.

Harwood, H.J., Jr. (2004). Acetyl-CoA carboxylase inhibition for the treatment of metabolic syndrome. Curr. Opin. Investig. Drugs *5*, 283–289.

Hedbacker, K., Birsoy, K., Wysocki, R.W., Asilmaz, E., Ahima, R.S., Farooqi, I.S., and Friedman, J.M. (2010). Antidiabetic effects of IGFBP2, a leptin-regulated gene. Cell Metab. *11*, 11–22.

Herzig, S., Long, F., Jhala, U.S., Hedrick, S., Quinn, R., Bauer, A., Rudolph, D., Schutz, G., Yoon, C., Puigserver, P., et al. (2001). CREB regulates hepatic gluconeogenesis through the coactivator PGC-1. Nature *413*, 179–183.

Herzig, S., Hedrick, S., Morantte, I., Koo, S.H., Galimi, F., and Montminy, M. (2003). CREB controls hepatic lipid metabolism through nuclear hormone receptor PPAR-gamma. Nature *426*, 190–193.

Hosooka, T., Noguchi, T., Kotani, K., Nakamura, T., Sakaue, H., Inoue, H., Ogawa, W., Tobimatsu, K., Takazawa, K., Sakai, M., et al. (2008). Dok1 mediates high-fat diet-induced adipocyte hypertrophy and obesity through modulation of PPAR-gamma phosphorylation. Nat. Med. *14*, 188–193.

Hughes, M.E., DiTacchio, L., Hayes, K.R., Vollmers, C., Pulivarthy, S., Baggs, J.E., Panda, S., and Hogenesch, J.B. (2009). Harmonics of circadian gene transcription in mammals. PLoS Genet. *5*, e1000442. 10.1371/journal.pgen.1000442.

Inoki, K., Kim, J., and Guan, K.L. (2011). AMPK and mTOR in cellular energy homeostasis and drug targets. Annu. Rev. Pharmacol. Toxicol. *52*, 381–400.

Kennedy, A.R., Pissios, P., Otu, H., Xue, B., Asakura, K., Furukawa, N., Marino, F.E., Liu, F.F., Kahn, B.B., Libermann, T.A., and Maratos-Flier, E. (2007). A high-fat, ketogenic diet induces a unique metabolic state in mice. Am. J. Physiol. Endocrinol. Metab. *292*, E1724–E1739.

King, D. (2011). The future challenge of obesity. Lancet *378*, 743–744.

Kohsaka, A., Laposky, A.D., Ramsey, K.M., Estrada, C., Joshu, C., Kobayashi, Y., Turek, F.W., and Bass, J. (2007). High-fat diet disrupts behavioral and molecular circadian rhythms in mice. Cell Metab. *6*, 414–421.

Koonen, D.P., Jacobs, R.L., Febbraio, M., Young, M.E., Soltys, C.L., Ong, H., Vance, D.E., and Dyck, J.R. (2007). Increased hepatic CD36 expression contributes to dyslipidemia associated with diet-induced obesity. Diabetes *56*, 2863–2871.

Kornmann, B., Schaad, O., Bujard, H., Takahashi, J.S., and Schibler, U. (2007). System-driven and oscillator-dependent circadian transcription in mice with a conditionally active liver clock. PLoS Biol. *5*, e34. 10.1371/journal.pbio.0050034.

Lamia, K.A., Storch, K.F., and Weitz, C.J. (2008). Physiological significance of a peripheral tissue circadian clock. Proc. Natl. Acad. Sci. USA *105*, 15172–15177.

Lamia, K.A., Sachdeva, U.M., DiTacchio, L., Williams, E.C., Alvarez, J.G., Egan, D.F., Vasquez, D.S., Juguilon, H., Panda, S., Shaw, R.J., et al. (2009). AMPK regulates the circadian clock by cryptochrome phosphorylation and degradation. Science *326*, 437–440.

Le Martelot, G., Claudel, T., Gatfield, D., Schaad, O., Kornmann, B., Sasso, G.L., Moschetta, A., and Schibler, U. (2009). REV-ERBalpha participates in

circadian SREBP signaling and bile acid homeostasis. PLoS Biol. *7*, e1000181. 10.1371/journal.pbio.1000181.

Lin, S., Thomas, T.C., Storlien, L.H., and Huang, X.F. (2000). Development of high fat diet-induced obesity and leptin resistance in C57Bl/6J mice. Int. J. Obes. Relat. Metab. Disord. *24*, 639–646.

Marcheva, B., Ramsey, K.M., Buhr, E.D., Kobayashi, Y., Su, H., Ko, C.H., Ivanova, G., Omura, C., Mo, S., Vitaterna, et al. (2010). Disruption of the clock components CLOCK and BMAL1 leads to hypoinsulinaemia and diabetes. Nature *466*, 627–631.

McTigue, K.M., Harris, R., Hemphill, B., Lux, L., Sutton, S., Bunton, A.J., and Lohr, K.N. (2003). Screening and interventions for obesity in adults: summary of the evidence for the U.S. Preventive Services Task Force. Ann. Intern. Med. *139*, 933–949.

Nakahata, Y., Sahar, S., Astarita, G., Kaluzova, M., and Sassone-Corsi, P. (2009). Circadian control of the NAD+ salvage pathway by CLOCK-SIRT1. Science *324*, 654–657.

Preitner, N., Damiola, F., Lopez-Molina, L., Zakany, J., Duboule, D., Albrecht, U., and Schibler, U. (2002). The orphan nuclear receptor REV-ERBalpha controls circadian transcription within the positive limb of the mammalian circadian oscillator. Cell *110*, 251–260.

Puri, V., Konda, S., Ranjit, S., Aouadi, M., Chawla, A., Chouinard, M., Chakladar, A., and Czech, M.P. (2007). Fat-specific protein 27, a novel lipid droplet protein that enhances triglyceride storage. J. Biol. Chem. *282*, 34213–34218.

Ramsey, K.M., Yoshino, J., Brace, C.S., Abrassart, D., Kobayashi, Y., Marcheva, B., Hong, H.K., Chong, J.L., Buhr, E.D., Lee, C., et al. (2009). Circadian clock feedback cycle through NAMPT-mediated NAD+ biosynthesis. Science *324*, 651–654.

Reddy, A.B., and O'Neill, J.S. (2010). Healthy clocks, healthy body, healthy mind. Trends Cell Biol. *20*, 36–44.

Rey, G., Cesbron, F., Rougemont, J., Reinke, H., Brunner, M., and Naef, F. (2011). Genome-wide and phase-specific DNA-binding rhythms of BMAL1 control circadian output functions in mouse liver. PLoS Biol. *9*, e1000595. 10.1371/journal.pbio.1000595.

Ruderman, N., Chisholm, D., Pi-Sunyer, X., and Schneider, S. (1998). The metabolically obese, normal-weight individual revisited. Diabetes *47*, 699–713.

Saltzman, E., Dallal, G.E., and Roberts, S.B. (1997). Effect of high-fat and low-fat diets on voluntary energy intake and substrate oxidation: studies in identical twins consuming diets matched for energy density, fiber, and palatability. Am. J. Clin. Nutr. *66*, 1332–1339.

Samuel, V.T., Liu, Z.X., Qu, X., Elder, B.D., Bilz, S., Befroy, D., Romanelli, A.J., and Shulman, G.I. (2004). Mechanism of hepatic insulin resistance in non-alcoholic fatty liver disease. J. Biol. Chem. *279*, 32345–32353.

Shaw, R.J., Lamia, K.A., Vasquez, D., Koo, S.H., Bardeesy, N., Depinho, R.A., Montminy, M., and Cantley, L.C. (2005). The kinase LKB1 mediates glucose homeostasis in liver and therapeutic effects of metformin. Science *310*, 1642–1646.

Talmud, P.J., Hawe, E., Martin, S., Olivier, M., Miller, G.J., Rubin, E.M., Pennacchio, L.A., and Humphries, S.E. (2002). Relative contribution of variation within the APOC3/A4/A5 gene cluster in determining plasma triglycerides. Hum. Mol. Genet. *11*, 3039–3046.

Turek, F.W., Joshu, C., Kohsaka, A., Lin, E., Ivanova, G., McDearmon, E., Laposky, A., Losee-Olson, S., Easton, A., Jensen, D.R., et al. (2005). Obesity and metabolic syndrome in circadian Clock mutant mice. Science *308*, 1043–1045.

Um, S.H., D'Alessio, D., and Thomas, G. (2006). Nutrient overload, insulin resistance, and ribosomal protein S6 kinase 1, S6K1. Cell Metab. *3*, 393–402.

Vollmers, C., Gill, S., DiTacchio, L., Pulivarthy, S.R., Le, H.D., and Panda, S. (2009). Time of feeding and the intrinsic circadian clock drive rhythms in hepatic gene expression. Proc. Natl. Acad. Sci. USA *106*, 21453–21458.

Wang, F., Liu, H., Blanton, W.P., Belkina, A., Lebrasseur, N.K., and Denis, G.V. (2010). Brd2 disruption in mice causes severe obesity without Type 2 diabetes. Biochem. J. *425*, 71–83.

Watanabe, M., Houten, S.M., Mataki, C., Christoffolete, M.A., Kim, B.W., Sato, H., Messaddeq, N., Harney, J.W., Ezaki, O., Kodama, T., et al. (2006). Bile acids induce energy expenditure by promoting intracellular thyroid hormone activation. Nature *439*, 484–489.

Zhang, E.E., Liu, Y., Dentin, R., Pongsawakul, P.Y., Liu, A.C., Hirota, T., Nusinow, D.A., Sun, X., Landais, S., Kodama, Y., et al. (2010). Cryptochrome mediates circadian regulation of cAMP signaling and hepatic gluconeogenesis. Nat. Med. *16*, 1152–1156.